


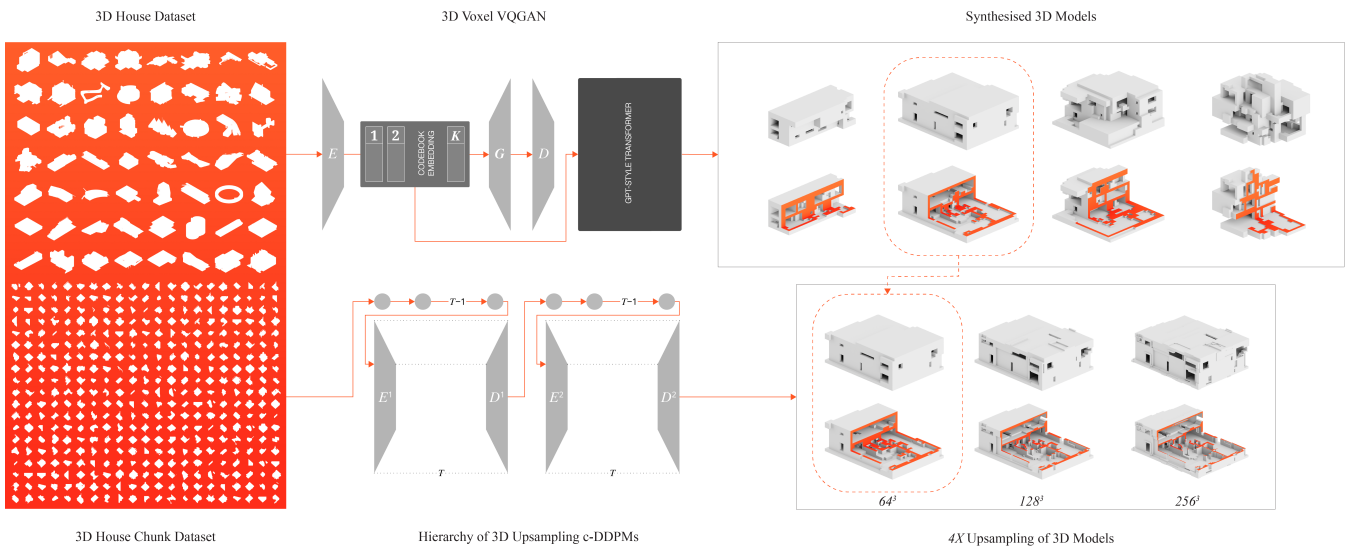


# ArchComplete: Autoregressive 3D Architectural Design Generation with Hierarchical Diffusion-Based Upsampling

S. Rasoulzadeh<sup>1</sup> , M. Bank Stigsen<sup>2</sup>, M. Wimmer<sup>1</sup> , I. Kovacic<sup>1</sup> , K. Schinegger<sup>2</sup>, S. Rutzinger<sup>2</sup>

<sup>1</sup> TU Wien, Center for Geometry and Computational Design, Austria

<sup>2</sup> University of Innsbruck, Department of Design, i.sd | Structure and Design, Austria



**Figure 1:** *ArchComplete* synthesises novel unseen coarse 3D models and augments them with fine geometric details to streamline the design process. Trained on a dataset of 3D house models, the 3D Voxel VQGAN whose composition is modelled with a transformer, generating models at a resolution of  $64^3$ . Thereafter, a set of 3D conditional Denoising Diffusion Models trained on cropped chunks, progressively generate higher-resolution grids in a coarse-to-fine manner up to resolution of  $256^3$ .

## Abstract

*ArchComplete* is a two-stage dense voxel-based 3D generative pipeline developed to tackle the high complexity in architectural geometries and topologies, assisting with ideation and geometric detailisation in the early design process. In stage 1, a 3D Voxel VQGAN model is devised, whose composition is then modelled with an autoregressive transformer for generating coarse models. Subsequently, in stage 2, Hierarchical Voxel Upsampling Networks consisting of a set of 3D conditional denoising diffusion probabilistic models are defined to augment the coarse shapes with fine geometric details. The first stage is trained on a dataset of house models with fully modelled exteriors and interiors with a novel 2.5D perceptual loss to capture input complexities across multiple abstraction levels, while the second stage trains on randomly cropped local volumetric patches, requiring significantly less compute and memory. For inference, the pipeline first autoregressively generates house models at a resolution of  $64^3$  and then progressively refines them to resolution of  $256^3$  with voxel sizes as small as 18cm. *ArchComplete* supports a range of interaction modes solving a variety of tasks, including interpolation, variation generation, unconditional synthesis, and two conditional synthesis tasks: shape completion and plan-drawing completion, as well as geometric detailisation. The results demonstrate notable improvements against state-of-the-art on established metrics.

## CCS Concepts

• **Computing methodologies** → **Artificial intelligence; Shape modeling;**

## 1. Introduction

Fields such as architecture, urban planning, or entertainment rely on high-quality three-dimensional models with rich geometric details and topology, which often require a significant amount of time, compute and memory to create. Volumetric design (also known as massing or schematic design) is usually the first and most important step in defining a design’s appearance. It begins by constructing rough 3D shapes within a defined design space before gradually refining them to include all the details needed for exterior and interior design elements [CCL\*21]. However, creating a good volumetric design requires a substantial amount of time and effort. Alternatively, a designer with a rough idea of the desired shape may quickly construct a coarse shape, to which a 3D generative model then adds realistic details. Such a generative pipeline capable of assisting the designer from the inception of an idea to its *geometry detailisation* has the potential to greatly simplify the design workflow.

In recent years, there has been a surge of new and exciting work on generative models for 3D shapes. These efforts are based on various frameworks and 3D geometric representations, achieving promising results in terms of quality and diversity [HLHF22, MCST22, CLT\*23, SAA\*24]. However, several challenges remain when adapting these methods to domain-specific design applications such as architecture, necessitating a tailored 3D generative pipeline addressing these challenges. Focusing on the architecture domain, first, there is a lack of detailed datasets of 3D models that encompass both exterior and interior spaces. Second, detailed 3D model of architectural buildings/houses are often more complex, or at least significantly different from the shapes in common 3D benchmark datasets like ShapeNet [CFG\*15] due to their structural and stylistic intricacies. Third, much of the literature on 3D generative models focuses on specific generation tasks, which cannot be easily extended to other downstream tasks (e.g., user editing), resulting in narrow application scopes. Additionally, compared to state-of-the-art 2D generative models for images, the additional third spatial dimension results in a dramatic increase in network parameters and memory-intensive feature maps in the 3D counterparts.

A 3D generative pipeline has to fulfil several criteria to accommodate the designers’ needs: (i) The design produced by the pipeline must maintain a 1:1 scale relative to the training data, ensuring consistency between the spatial characteristics of the models (such as openings and room heights in the architectural domain); (ii) The generative pipeline should be capable of synthesizing realistic, high-fidelity models while aiding designers in quickly exploring the design space with flexible and interactive use and refinement: For example, a designer may want to blend input models from different distinct styles to create an intermediate model (*aka* shape interpolation), generate versions with varying details, or may provide partially modelled input asking for completion suggestions, i.e., shape completion. (iii) Or an artist may provide coarse shapes, thereby guiding the pipeline to create large varieties of fine and detailed geometries through a process referred to as *geometry detailisation*.

To address the identified challenges, we propose *ArchComplete*, a voxel-based 3D generative pipeline operating in two stages: a

*Base Network* for coarse shape ideation and *Hierarchical Upsampling Networks* for augmenting the shapes with fine geometric details (see Figure 1). To overcome the lack of architectural datasets, the first dataset of 3D house models featuring fully modelled exteriors and interiors is introduced. Inspired by recent advancements in generative models for images [ERO21] and natural language [LSC24], we adopt a sequence-based approach to synthesise voxelised models as a sequence of local volumetric patches. A 3D Vector-Quantised Generative Adversarial Network *3D Voxel VQGAN* is designed to encode voxelised models into latent quantised embeddings by learning a vocabulary of patches. To better capture geometric and topological features at the scale of local patches, we introduce a novel 2.5D perceptual loss and employ 3D PatchGAN as the discriminator. We model our 3D Voxel VQGAN’s composition with a transformer that learns statistical correlations between patches enabling autoregressive generation of local patch sequences forming a 3D voxelised model. The transformer’s integration enables a range of interaction modes, addressing the required flexibility in downstream tasks. In the second stage, we aim to push the limits of purely 3D generative priors for high-resolution shape generation in dense voxel-based methods while alleviating high computational demands. To this end, we define a hierarchy of 3D conditional Denoising Diffusion Probabilistic Models (*3D c-DDPMs*) [HJA20] that train on local chunks instead of the entire 3D voxelised models and upsample the coarse outputs from the first stage into finer grids. This hierarchical upsampling strategy mitigates ambiguity in voxel upsampling with large rates by introducing intermediate-level supervision while making distribution at each level easier to model since the coarse levels model rough patches and finer levels focus on local details.

We demonstrate the versatility of our pipeline in the 3D architectural modelling domain through several example applications. These include leveraging Genetic Algorithm (GA) operators to generate endless interpolations and variations of synthesised models. Additionally, we explore unconditional synthesis and two conditional synthesis tasks, shape completion and plan-drawing completion, highlighting their potential in architectural modelling. Finally, quantitative and qualitative evidence is provided showing that ArchComplete outperforms prior methods in both unconditional and conditional synthesis tasks based on established metrics.

Code and dataset are available at: <https://gitlab.cg.tuwien.ac.at/srasoulzadeh/archcomplete.git>

## 2. Related Work

Unlike 2D images, it is less clear how to represent 3D data effectively. Various representations with pros and cons have been explored, particularly when considering 3D generative models. For instance, quite a large number of 3D generative models have been developed for point clouds [ADMG18, LH21], dense voxel grids [LYF17] and more recently, sparse voxel grids [SSN\*22, RHZ\*24], meshes [SAA\*24], and signed distance functions (SDFs) [MCST22, HLHF22, CLT\*23], etc. In this work, given our target task, i.e. volumetric design, we opted to use a simple and plain explicit dense voxel grid representation, as it directly corresponds to the representation of volume in 3D space. It shares a similar form with 2D pixels, facilitating the adoption of various

image generation methods that have not been extensively explored in this domain. However, it is noteworthy that the dense nature of voxels results in increased computational resources and time requirements when generating high-resolution shapes, necessitating ingenious strategies to address these challenges.

Herein, since both voxel grids and Truncated Signed Distance Functions (TSDFs) represent 3D space in voxels, with the former storing binary occupancy values and the latter storing the truncated scalar distances to the nearest surface, we will review a few state-of-the-art 3D generative and diffusion models that adopt these two representations and learn based on them while paying particular attention to their use in synthesis within the 3D architectural domain.

**3D Generative Models.** Numerous 3D generative models build on various frameworks, including generative Variational Auto Encoders (VAEs) [DMVPSC19, GJvK20, SHR23], Generative Adversarial Networks (GANs) [LYF17, WSH\*18, WZ22], Graph Neural Networks (GNNs) [ZKF23, BDEW], and Auto Regressive (AR) models [MCST22, SAA\*24]. In [DMVPSC19], within the architectural domain, the VAE introduced in [Kin13] is employed for the generation, manipulation, and form-finding of building typologies represented as voxelised wireframes. Another work with architectural design use cases is [SHR23], which employs a Conditional Variational Auto Encoder (cVAE) trained on voxelised data, coupled with corresponding operative verbs (a taxonomy of simple geometrical operations) in a prototype of a generative volumetric design tool.

Our pipeline’s first network is built upon [VDOV\*17] and inspired by a later proposed method VQGAN [ERO21]. [VDOV\*17] first proposed a method to learn quantised and compact latent representations for 2D images using the Vector-Quantized Variational AutoEncoder (VQVAE), and later introduced a hierarchical version [RVdOV19]. Followingly, VQGAN [ERO21] learns autoregressive generation over the discrete VQVAE representations by integrating a mask generative Transformer through discrete semantic codebooks. Our work utilises VQGAN’s network design as its backbone and extends it to the domain of 3D voxelised shapes in architectural design. It also integrates a new loss term affecting the cohesiveness and integrity of the generated 3D house models.

**3D Diffusion Models.** Diffusion Probabilistic Models (DPMs) [HJA20], also known as Diffusion Models, have currently arisen as a powerful family of generative models. In the fields of computer graphics and vision, several recent studies have adopted diffusion models for generative 3D modelling [HLHF22, VWG\*22, LDZL23, SÖLH23, SCP\*23, RHZ\*24, WLY\*24]. Existing approaches mostly train a VQ-VAE on a 3D representation like voxel grids, SDFs, and Triplanes, and then employ a diffusion model in the learned latent space. NWD [HLHF22] encodes 3D shapes by building a compact wavelet representation with a pair of coarse and detail coefficient volumes through TSDF decomposition. It then formulates two networks upon on DPMs to generate shapes in the form of coarse and detail coefficient volumes for generating shapes and reconstructing fine details, respectively. LION [VWG\*22] uses a VAE framework with hierarchical DDMs in latent space that combines a global shape latent representation with a point-structured latent space, and integrates it with Shape as Priors (SAP) [PJL\*21] for

mesh generation. Diffusion-SDF [LDZL23] presents a two-stage pipeline comprising a patch-wise autoencoder and a voxelised diffusion model to generate voxelised SDFs conditioned on texts. On the other hand, NFD [SCP\*23] is another diffusion-based 3D generative model that, instead of voxel grids, converts the occupancy field of an object in a set of axis-aligned triplane feature representations.

### 3. Dataset

The current state of available 3D datasets such as BuildingNet [SNL\*21], Houses3K [PCN\*20] or 3DBAG [BAG24] presents limitations for architectural design applications. They are either inconsistent in labelling or lack a consistent degree of detail with modelled interiors for generating detailed building design [WDL\*23]. Comprehensive 3D datasets, especially those depicting both exterior and interior details of buildings, are therefore particularly valuable as they provide a complete representation of the spatial relations architects and designers envision.

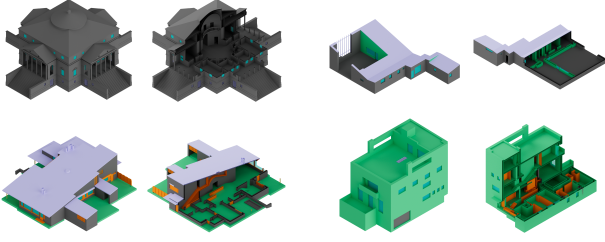
To this end, we adopt our own collected dataset consisting of 1500 3D house models, including both the original and augmented samples that depict prominent architectural houses with fully modelled interiors and material labels, as showcased in Figure 2. The dataset aims to address the aforementioned significant challenge in the literature: the lack of high-quality publicly available 3D architectural datasets that fully capture spatial relations. The dataset was curated specifically to overcome these limitations by offering detailed 3D architectural models that capture the nuanced relationships between spatial configurations, structural integrity, and materiality—critical elements in the architectural design process. Additionally, a key aspect of this dataset is that it consists of architectural precedents—pre-existing buildings/houses or projects that serve as inspiration for new designs. These precedents provide both explicit and implicit knowledge on how past design challenges related to spatial organisation and aesthetics [Cro82], making the dataset a valuable resource for 3D generative models for learning purposes. The original samples in the dataset were collected through structured research-led teachings at University of Innsbruck, where architecture students were tasked with modelling existing houses as part of the curriculum in both past and ongoing courses.

For detailed information on the augmentation techniques used to expand the dataset, please refer to the Supplementary Material.

### 4. Method

The framework of our voxel-based 3D pipeline generates designs for both early-stage design ideation and subsequent geometric detailisation of the designs. It operates in two main stages: A base network for coarse model generation and hierarchical upsampling, augmenting the design with fine geometric details. The following major procedures define the pipeline:

- (i) *Data Preparation*, to construct the ground-truth data for the pipeline’s two stages, and defining the input/output of each stage using a collected dataset of 3D house models.
- (ii) *A Base Network*, generating coarse voxelised models by leveraging a patch-wise quantisation step along with a Transformer-



**Figure 2:** Example 3D houses of the dataset. The geometry is sliced with two cutting planes to reveal its corresponding interior. Individual colours are representative of different materials.

based autoregressive model (see Figure 3 (a)). Following VQGAN [ERO21], we define a 3D Voxel VQGAN to learn discrete representation of the data. Different from base VQGAN, a new 2.5D perceptual loss is introduced within the encoding to enhance semantic understanding and extract geometrically rich features that capture intricate details of models. Trained on voxelised house models in our dataset, we first learn a vocabulary of geometric embeddings corresponding to local patches in the models, enabling them to be encoded and decoded from the embeddings. The learned embeddings are then used to train a transformer to reconstruct masked input sequences. At inference, the transformer autoregressively predicts patch embeddings, which are decoded to generate diverse and novel voxelised models.

- (iii) *Hierarchical Voxel Upsampling Networks* consisting of a set of 3D conditional denoising diffusion models that generate progressively higher resolution models in a feed-forward fashion (See Figure 3 (b)). At each level, the model is trained on pairs of local coarse and fine patches extracted from the collection of voxelised house models, with the coarse patches serving as a conditioned 3D prior to guide the generation of finer outputs. In essence, for each pair, the model learns by iteratively subdividing coarse patches into octants and pruning excessive ones in the denoising process. Our current implementation defines a three-level hierarchy, where during inference, the voxel grids from the prior stage are unfolded into local patches, progressively upsampled, and then folded back to produce a higher-resolution voxel grid with a 4X upsampling rate.

#### 4.1. Data Preparation

Prior to voxelising our data samples, as part of pre-processing, we filter out openings in the house dataset geometries, i.e., parts labelled as doors and windows, to focus solely on the mass-void relationship (closed and open spaces). Additionally, we remove parts labelled as ground to attend exclusively to the structural components of the models. We then concentrate solely on the dense binary voxelisation of data samples, where each voxel contains a value of either 0 or 1, representing an empty (void) or occupied voxel (mass), respectively, while leaving the integration of materials and semantics for future work.

In order to create ground-truth for our base 3D Voxel VQGAN

network, we take the models in their original 1:1 scale, limit ourselves to the design space of  $48\text{m}^3$ , and voxelise only the regions of the models falling within this space at a resolution of  $64^3$ , resulting in a voxel size as small as 75cm. In total, we end up with 1500 voxelised models ready for training our Base Network.

To build the ground-truth voxel hierarchy of local chunks for training our Hierarchical Upsampling Networks, we sample 100 approximately equidistant points using Poisson disk sampling [Yuk15] on the surface of each model from dataset. Then, similar to the data preparation for training for the 3D Voxel VQGAN, we crop chunks at a size of  $6\text{m} \times 6\text{m} \times 6\text{m}$ , centred at the sampled points, and voxelise them into three different resolutions:  $8^3$ ,  $16^3$  and  $32^3$ , as illustrated in Figure 4. This results in two pairs of 12500 pair of coarse and fine chunks to train each hierarchy level of our 3D upsampling c-DDPMs. The intuition behind this is that since the dataset models exhibit interior and exterior structures, each chunk is geometrically self-contained. Training the upsampling networks on local chunks alleviates the need for high computational resources due to their much lower resolutions.

## 4.2. Base Network: 3D Voxel VQGAN

### 4.2.1. Learning Quantised Voxel Grid Embeddings

We extend the original 2D VQGAN [ERO21] to the 3D Voxel VQGAN by making three key modifications: (i) we utilise 3D volumetric residual blocks as the backbone of its encoder  $E$  and decoder  $G$ , extending them to 3D; (ii) we replace the original discriminator with a 3D PatchGAN [IZZE17], enforcing fidelity at the scale of local volumetric patches; and (iii) we incorporate a 2.5D perceptual loss term, pushing the network to learn both local fine-grained details and global arrangement of voxels within a grid.

Given an input model, represented via a binary voxel grid  $v \in \{0, 1\}^{R \times R \times R}$ , we have

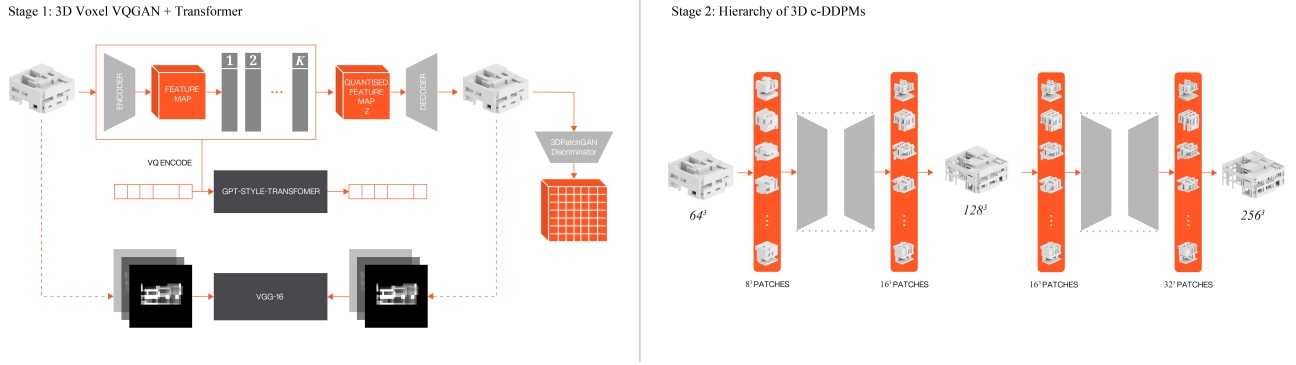
$$z = \text{VQ}(E(v)), \quad \text{and} \quad \hat{v} = G(z), \quad (1)$$

where  $z \in \mathbb{R}^{r \times r \times r \times D}$  is the latent feature map of  $E$  with dimension  $r < R$  and VQ is the quantisation step which maps each of the  $r^3$   $D$ -dimensional vectors of the latent feature map to their nearest vector in the discrete codebook  $\mathcal{C} = \{z_k | z_k \in \mathbb{R}^D\}_{k=1}^K$ . In other words, the original input voxel grid is encoded into  $D$ -dimensional embeddings each determining a  $r^3$  local patch in the original voxel grid.

The original vanilla VQGAN is trained by optimising a vector quantised codebook during autoencoding with the discriminator optimised to differentiate between real and reconstructed inputs. Denoting the reconstructed voxel grids with  $\hat{v}$ , the overall loss of vanilla VQGAN can be written as:

$$\underbrace{\|v - \hat{v}\|}_{\mathcal{L}_R} + \underbrace{\|\text{sg}[E(v)] - z_q\|_2^2 + \|\text{sg}[z_q] - E(v)\|}_{\mathcal{L}_C} + \underbrace{[\log D(v) + \log(1 - D(\hat{v}))]}_{\mathcal{L}_D}, \quad (2)$$

where  $\text{sg}[\cdot]$  denotes the stop-gradient operation and  $\mathcal{L}_R$ ,  $\mathcal{L}_C$ , and  $\mathcal{L}_D$  are the reconstruction, the so-called "commitment", and the discriminator losses, respectively. However, when extending to 3D



**Figure 3: Pipeline Overview.** The framework follows a two-stage 3D generative pipeline: In stage 1, a 3D Voxel Vector-Quantised Generative Adversarial Network (3D Voxel VQGAN) is trained on a dense voxel-based representation of our data to learn a patch-wise quantisation to learn the vocabulary of the local volumetric patches. A transformer is then used to generate 3D models as sequences of token indices derived from the pre-learned codebook’s patch-wise vocabulary. In stage 2, a hierarchical upsampling strategy is employed consisting of a set of 3D conditional Denoising Diffusion Probabilistic Models (3D c-DDPMs). These models learn a hierarchy of local volumetric patches conditioned on coarser levels in a cascaded fashion. During inference, the coarse model is unfolded into patches and conditioned for upsampling, upsampled to 2X resolution, and folded back to generate twice higher resolution grid, respectively. This process continues until the highest desired resolution is achieved. The current implementation experiments with a 4X upsampling rate.

voxel grids, capturing perceptually rich codebook vectors that reflect spatial and structural relationships in complex inputs like 3D buildings as bona fide geometric objects necessitates going beyond mere voxel-wise matching as in  $\mathcal{L}_R$ . To this end, we propose a 2.5D perceptual loss

$$\mathcal{L}_P^{2.5}(v, \hat{v}) = \frac{\sum_{i \in \{x, y, z\}} \sum_j \lambda_j \|\phi_j(S_i(v)) - \phi_j(S_i(\hat{v}))\|}{3}, \quad (3)$$

where  $\phi_j$  represents the individual layers of a pre-trained visual perception network, specifically VGG-16 [SZ14]), and  $S_i$  is a slicing function that slices the input 3D voxel grid along its  $i$ -th axis ( $x$ ,  $y$ , or  $z$ ), and then spatially averages resultant 2D axial images. In other words, the term  $\mathcal{L}_P$  essentially enables capturing correspondence between the reconstructed and ground-truth grids at increasing levels of abstraction. Moreover, we also employ a 3D PatchGAN to distinguish real and reconstructed voxel grids at the scale of  $R_D \times R_D \times R_D$  patches where  $R_D < R$ .

The final loss function  $\mathcal{L}_{3D\text{VoxelVQGAN}}$  is a weighted sum of the individual loss terms:

$$\mathcal{L}_{3D\text{VoxelVQGAN}} = \alpha \mathcal{L}_R + \beta \mathcal{L}_P^{2.5} + \gamma \mathcal{L}_C + \delta \mathcal{L}_D. \quad (4)$$

An ablation study is conducted to provide deeper insights into the role of the 2.5D perceptual loss (refer to the Supplementary Material).

#### 4.2.2. Learning the Composition of Voxel Grids with Transformers

With  $E$  and  $G$  available, we can now represent the voxel grids in terms of the sequence of codebook-index tokens of their encodings. The quantised encoding of a voxel grid  $v$  given by  $z = \text{VQ}(E(v)) \in \mathbb{R}^{r \times r \times r \times D}$ , is equivalent to sequence  $s \in \{0, \dots, K\}^{r \times r \times r}$  of indices

from the codebook obtained by replacing each code by its index in the codebook  $\mathcal{C}$ :

$$s_{uvw} = k \quad \text{such that} \quad (z)_{uvw} = z_k. \quad (5)$$

By mapping indices of a sequence  $s$  back to their corresponding codebook entries,  $z = (z_{s_{uvw}})$  is readily recovered and decoded to a voxel grid  $\hat{v} = G(z)$ .

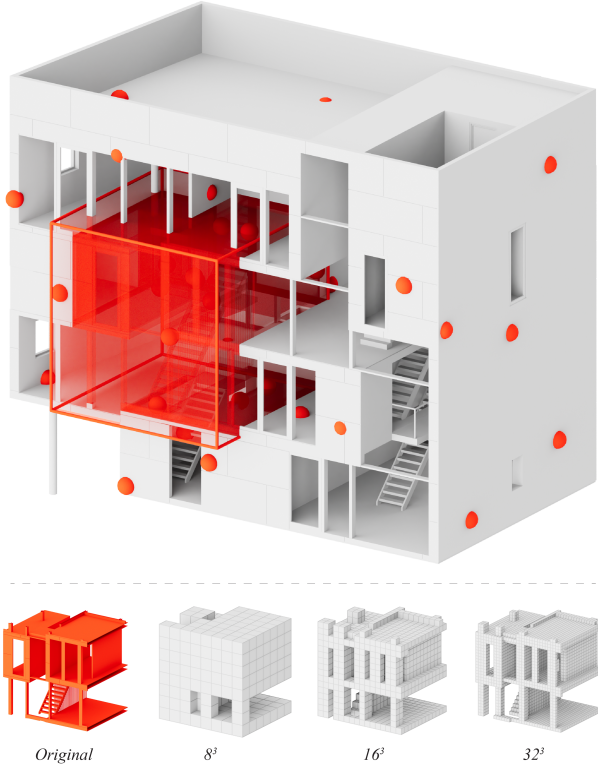
Thus, after choosing some ordering of the indices in  $s$  of samples in the training dataset, voxel grid generation can be formulated as an autoregressive next-index prediction task. More precisely, given indices  $s_{<i}$ , a transformer can be learned to predict the distribution of possible following indices, i.e.  $p(s_i | s_{<i})$  to compute the likelihood of the full representation  $p(s) = \prod p(s_i | s_{<i})$ . Essentially, this allows us to directly maximise the log-likelihood of the data representations:

$$\mathcal{L}_{3D\text{VoxelVQGAN\_TRANS}} = \mathbb{E}_{v \sim p(v)} [-\log p(s)]. \quad (6)$$

To this end, we prefix the sequences with a start of sentence (*SOS*) token and employ a decoder-only transformer architecture, specifically a miniature version of original GPT model [Rad18]. Our customised architecture of this model begins with an embedding layer for encoding (indices) tokens and their corresponding positions and then the features pass through a stack of multi-headed self-attention layers, followed by a small-sized MLP trained to predict the codebook index of the next embedding in the sequence.

#### 4.2.3. Regularising Voxel Grids

The raw voxel grid outputs of the 3D Voxel VQGAN may contain artefacts, such as voxels either sticking out from the model’s surface or floating in space. To clean up the voxel grid, we devise an algorithm that considers the connectivity between mass (1) and



**Figure 4:** Sampling chunks on a 3D house model and the corresponding voxelisation in three different resolutions forming the ground-truth data for training hierarchical upsampling networks. Not all 100 points are shown due to visual ease.

void (0) voxels and compute the contribution of each voxel to the artefacts. To this end, we define the *Variation Contribution* ( $V_c$ ) of each voxel as the sum of the  $L_1$  distances between it and its adjacent voxels along the three axes. In this setting, voxels sticking out have  $V_c = 4$  or  $V_c = 5$ , while floating voxels have  $V_c = 6$ . We iteratively mask out these voxels while retaining the remaining ones in the grid, eventually resulting in a clean, artefact-free voxel grid (refer to the pseudocode in Algorithm 1).

#### 4.3. Hierarchical Voxel Upsampling Networks: 3D c-DDPMs

Our method for refining dense voxel grids from a prior step into higher-resolution grids trains a hierarchy of 3D conditional Denoising Probabilistic Diffusion Models (3D c-DDPMs) on a hierarchy of coarse-to-fine chunks extracted from the raw dataset samples. The hierarchy comprises  $L$  levels of coarse-to-fine chunks  $\mathcal{C} = \{C_1, \dots, C_L\}$ , where each chunk in the finer level  $C_{l+1}$ , is strictly contained within its corresponding chunk in the coarser level  $C_l$  for  $l = 1, \dots, L-1$ , and the finest chunks,  $C_L$ , contain the maximum amount of detail.

The typical denoising probabilistic diffusion is a purely generative model that takes no conditioning input and consists of a *for-*

---

#### Algorithm 1 Voxel Grid Clean-Up Method

---

```

1: Input:  $v$ : Input Voxel Grid,  $N$ : Number of iterations
2: Output:  $v_{\text{clean}}$ : Output Cleaned-Up Voxel grid
3: for  $i = 1$  to  $N$  do
4:   # Compute voxel differences:
5:    $V_{c_1} \leftarrow \sum_{d=1}^{D-1} \sum_{h=1}^H \sum_{w=1}^W |v_{d+1,h,w} - v_{d,h,w}|$ 
6:    $V_{c_2} \leftarrow \sum_{d=1}^D \sum_{h=1}^{H-1} \sum_{w=1}^W |v_{d,h+1,w} - v_{d,h,w}|$ 
7:    $V_{c_3} \leftarrow \sum_{d=1}^D \sum_{h=1}^H \sum_{w=1}^{W-1} |v_{d,h,w+1} - v_{d,h,w}|$ 
8:    $V_c \leftarrow V_{c_1} + V_{c_2} + V_{c_3}$ 
9:   # Create mask  $M$ :
10:  if  $V_c(d, h, w) \neq 4$  and  $V_c(d, h, w) \neq 5$  then
11:     $M(d, h, w) \leftarrow 1$ 
12:  else
13:     $M(d, h, w) \leftarrow 0$ 
14:  end if
15:  # Element-wise multiplication
16:   $v \leftarrow v \odot M$ 
17: end for
18:  $v_{\text{clean}} \leftarrow v$ 
19: Return  $v_{\text{clean}}$ 

```

---

*ward* and a *reverse* process. During the forward phase, a sample is corrupted by adding noise in a step-wise manner, where the noise-adding process forms a Markov chain. Contrarily, the reverse phase recovers the corrupted data at each step with a denoising model.

*Forward Process:* Given a sample  $x_0 \sim q(x_0)$ , the forward Markov process  $q(x_{1:T}|x_0) = \prod_t q(x_t|x_{t-1})$  corrupts the sample into a sequence of increasingly noisy samples:  $x_1, \dots, x_T$ , where  $t$  refers to the diffusion step. Generally, the noise follows a Gaussian distribution:  $q(x_t|x_{t-1}) = \mathcal{N}(x_t|x_{t-1}; \sqrt{1 - \beta_t}x_{t-1}, \beta_t \mathbf{I})$  where  $\beta_t$  is the scale of the added noise at step  $t$ .

*Reverse Process:* The reverse Markov process attempts to recover the last-step sample with a parametrised denoising model  $p_\theta(x_{t-1}|x_t)$ . When the noise follows a Gaussian distribution, the parameterised distribution becomes

$$p_\theta(x_{t-1}|x_t) = \mathcal{N}(x_{t-1}|\mu_\theta(x_t, t), \sigma_\theta(x_t, t)) \quad (7)$$

where  $\mu_\theta(x_t, t)$  and  $\sigma_\theta(x_t, t)$  are modelled with neural networks.

The vanilla DDPM functions as an unconditional generative model. However, in our case, coarse chunks  $C_i$  can provide additional context or guidance during the reverse denoising process. To this end the underlying U-Net architecture [RFB15] is modified slightly by utilising 3D residual blocks and changing the network architecture to accept three inputs: the coarse chunks  $C^l$ , fine chunks  $C^{l+1}$ , and time step  $T$ . This is achieved by adding an additional layer, which concatenates the subdivided coarse and the fine voxel grid in the input layer. In our 3D conditional DDPM setup, the forward process remains almost the same, within which Gaussian noise is progressively added to the fine chunks  $C^{l+1}$ , at times  $t \in \{1, \dots, T\}$ :

$$q(C_t^{l+1}|C_{t-1}^{l+1}) := \mathcal{N}(C_t^{l+1}; \sqrt{1 - \beta_t}C_{t-1}^{l+1}, \beta_t \mathbf{I}). \quad (8)$$

The purpose of subdividing the coarse chunks is to match the resolution of the fine ones, thereby guiding the denoising process

in the removal of extra occupied voxels, ultimately resulting in a finer chunk with higher resolution.

Symmetrically, the reverse process modifies the Equation 7 by conditioning it on the coarse chunks  $C^l$  to help the model generate higher resolution chunks that are consistent with the coarse ones

$$p_{\theta}(C_{t-1}^{l+1}|C^l, C_t^{l+1}) = \mathcal{N}(\mathbf{x}_{t-1}; \mu\theta(\mathbf{x}_t, t, \mathbf{c}), \Sigma\theta(\mathbf{x}_t, t, \mathbf{c})). \quad (9)$$

Notably, this posterior can be used to generate fine chunks given conditioned coarse chunks and the Gaussian noise  $\mathcal{N}(0, \mathbf{I})$  by reducing the noise gradually from timestep  $T$  to 0.

Once the diffusion models  $p_{\theta_l}$ , for  $l = 1, \dots, L-1$  are learned as described above, for using it throughout the inference phase, the input voxel grid is first unfolded into the chunks at the coarsest scale. Then, the decoder of the  $p_{\theta_1}$  is used to upsample the grid’s constituent chunks  $C^1$  to  $\hat{C}^2$ . Conditioned on  $\hat{C}^2$ , the diffusion model  $p_{\theta_2}$  is used to generate chunks  $\hat{C}^3$  for the next level, and the process continues until the chunks at the highest resolution,  $\hat{C}^L$ , are obtained. Finally, the high-resolution chunks are folded back, resulting in an output voxel grid with a resolution  $2^{L-1}$  times higher, exhibiting finer geometric details.

#### 4.4. Implementation Details

We implement our networks using TensorFlow and run all experiments on a GPU cluster with two Nvidia A100 GPUs. In learning the VQGAN’s codebook vectors, we set the resolution of the latent feature map  $r = 8$ , with the codebook constituting  $K = 512$ ,  $D = 128$ -dimensional vectors. Our 3D PatchGAN discriminator has a receptive field of  $R_D = 8$ . As for the loss weight factors, we set  $\alpha = 100$ ,  $\beta = 10$ , according to our ablation study (refer to supplementary Material for further details). We set  $\lambda$  and  $\delta$  to 0.25 and 0.1, respectively, following the vanilla 2D VQGAN [ERO21] implementation. The base network is trained utilising the Adam optimiser [Kin14] with the learning rate of  $10^{-4}$ , while simultaneously the discriminator is trained with the learning rate of  $10^{-6}$  for 128 epochs with an effective batch size of 4. For our transformer, we use a miniature GPT model equipped with a context window of up to 512 embeddings. We use AdamW optimiser [Los17] with cosine annealing strategy [LH16] with minimum and maximum learning rates of  $10^{-5}$  and  $2.5 \times 10^{-4}$ , for 128 epochs with a batch size of 32.

For the hierarchical upsampling networks (3D c-DDPMs), we follow the same setup for training the vanilla diffusion model. We use Adam optimiser with the learning rate of  $10^{-4}$ , for 256 epochs with a batch size of 32. For inference, we use DDIM [SME20] as our sampler with the number of timesteps  $T = 100$ .

For details of the networks’ architectures, please refer to the Supplementary Material.

## 5. Results and Validation

In this section, we first present several example applications of our pipeline (Section 5.1) and subsequently evaluate various aspects of the pipeline in comparison with state-of-the-art methods. (Section 5.2).

### 5.1. Example Applications

We conduct comprehensive experiments to showcase different applications of ArchComplete. We draw inspiration from Genetic Algorithm (GA) operators and apply them to codebook tokens to generate interpolations (blendings) and variations of input house models to facilitate ideation based on existing 3D models. After that, using the autoregressive model trained to predict the learned codebook indices, we demonstrate both unconditional and two conditional 3D generation tasks. For the conditional case, we utilise an existing 3D voxel creation interface to demonstrate the pipeline’s application to plan-drawing completion, a newly formulated architecture-specific use-case of ArchComplete.

#### 5.1.1. GA-Inspired Interpolation & Variation

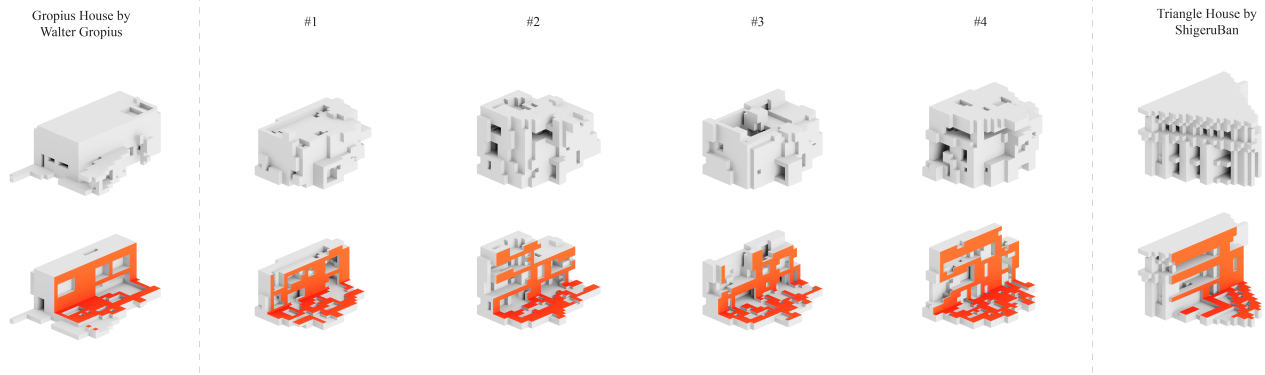
The quantisation process transforms the input model into a discrete set of index tokens corresponding to specific codebook vectors. Consequently, the challenge of shape interpolation or shape variation can be reframed as a well-defined problem in this discrete space, which can be effectively addressed using two genetic algorithm (GA) operators: crossover and mutation.

**Blending.** Consider two sets of codebook token sequences  $z_1$  and  $z_2$  corresponding to encoding of two different input models. Using a random uniform crossover, we create an interpolated token sequence  $z_{\text{int}}$  by randomly selecting each token from  $z_1$  or  $z_2$  randomly with equal probability, i.e. 0.5. This essentially entails mixing the tokens corresponding to embeddings of local patches in the two models. When decoded using  $G$ ,  $z_{\text{int}}$  produces an interpolated shape inheriting characteristics from both original input models (see Figure 5).

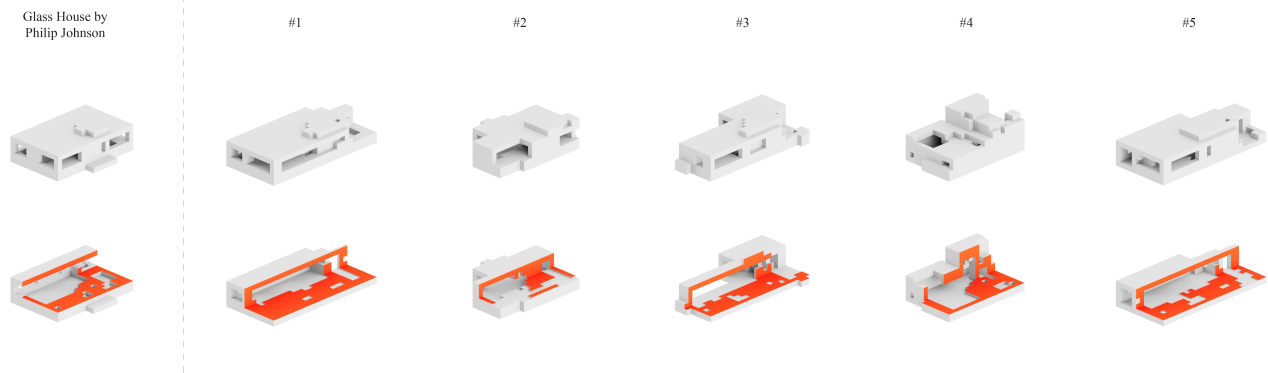
**Variation.** Similarly, variations of each input model can be generated by applying mutation operators to its token sequence. The mutation alters certain tokens, resulting in distinct model variants upon decoding. To this end, we use swap mutation, which randomly selects and swaps two tokens iteratively. Given a sequence of codebook index  $z$ , we repeat this process 128 times—one-fourth of the sequence length—as we found this to introduce diversity without heavily distorting the input (see Figure 6).

#### 5.1.2. Unconditional Synthesis

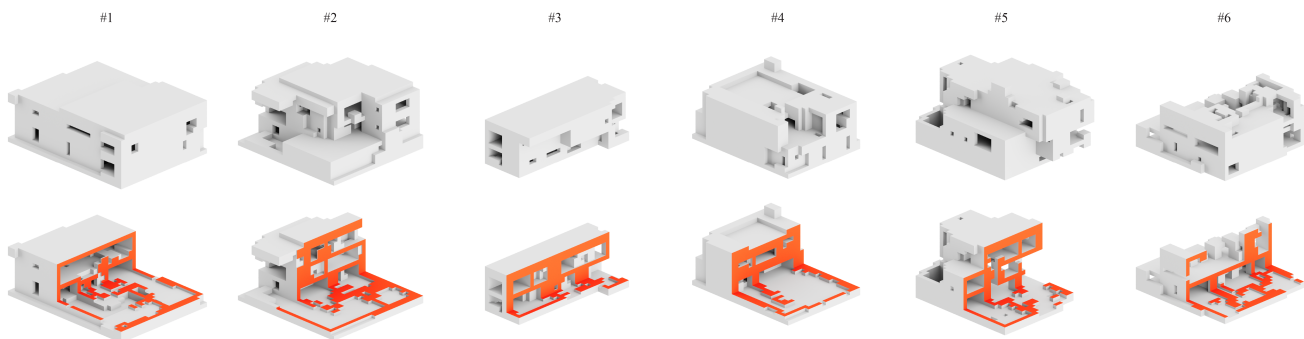
Given a transformer trained to autoregressively predict token sequences, generating novel, unseen outputs without any given prior context—*aka* unconditional synthesis—becomes a straightforward task. To this end, as a convention in the ordering of generation, we start with the SOS token and iteratively sample new tokens, each conditioned on the previously generated tokens. This process continues until the sequence reaches its maximum length, which is equal to the size of the output feature map from the encoder, i.e.  $r \times r \times r$  which is equal to  $512 = 8 \times 8 \times 8$  (see Section 4.2.1 and 4.2.2). Afterwards, by retrieving the corresponding codebook vectors and performing quantisation, we use the decoder to generate the novel house models (see Figure 7). The unconditionally synthesised outcomes illustrate the model’s capacity to suggest architectural diverse and coherent houses which differ from the training data.



**Figure 5:** Four interpolated house shapes created by blending two input house models. The interpolations are generated by applying crossover operations on the corresponding token sequences of the input models.



**Figure 6:** Five variations of an input house model generated using the swap mutation applied to codebook tokens, demonstrating how this operation creates multiple variations that retain similarities to the original 3D model while introducing distinct changes.

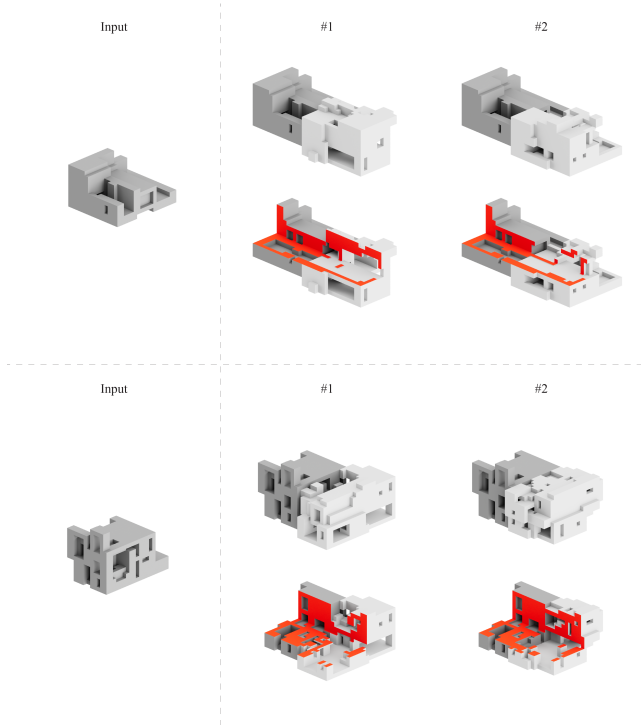


**Figure 7:** Six unconditionally synthesised 3D houses using the transformer trained on codebook tokens.

### 5.1.3. Conditional Synthesis

Thanks to the autoregressive structure of our transformer, conditioning can be achieved by simply providing a partial sequence



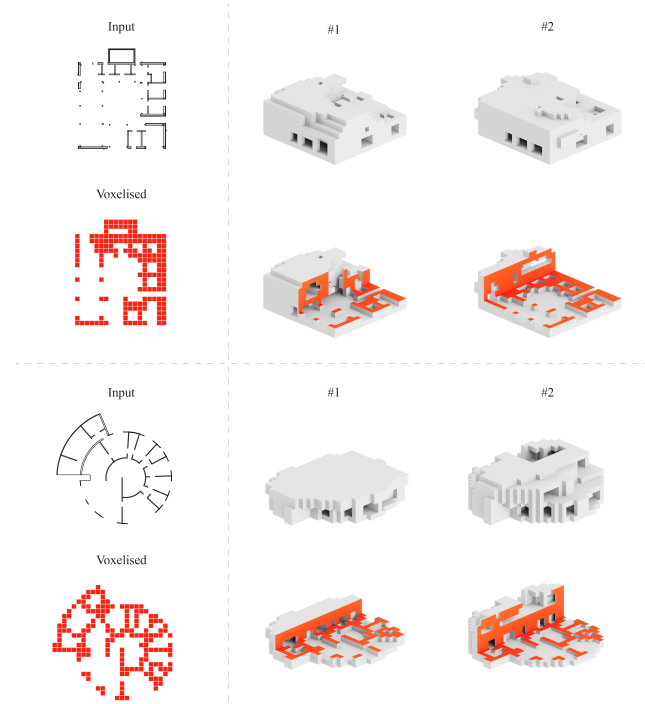


**Figure 8:** The model can infer multiple possible completions for a given partial shape of a house model, leveraging its probabilistic nature to generate diverse shape hypotheses.

corresponding to the partial observation and generating completions by sequentially sampling the next token until the maximum sequence length is reached. In the following sections, we explore two graphics applications that can support designers with ideation during early-stage 3D architectural design.

**Shape Completion** Given a partially modelled input, our model can infer multiple possible completions and provide them as suggestions to the designer. To mimic such a scenario, we create a partial sample by employing a block mask on half of an unseen voxel grid of a house model and use the transformer to sample the remaining token sequences to illustrate our model’s partial completion capabilities (see Figure 8). The shown completions highlight how the model can suggest solutions that are in coordination with the partial one.

**Plan-Drawing Completion** A unique application of shape completion that benefits ideation in architectural design is plan-drawing completion. It allows designers to draw a 2D plan of their intended designs and ask the pipeline for the complete model. We demonstrate this capability by asking users to create and edit their desired floor plans from a top-view on a 2D plane in Goxel [Che24], a Minecraft-style 3D voxel editor. Figure 9 shows two examples of how plan drawing completions can be inferred from voxelised input drawings, highlighting how such a completion capability can integrate into traditional architectural ideation workflows.



**Figure 9:** Two examples of how the model can infer multiple possible completions based on a voxelised drawing of an input floor plan.

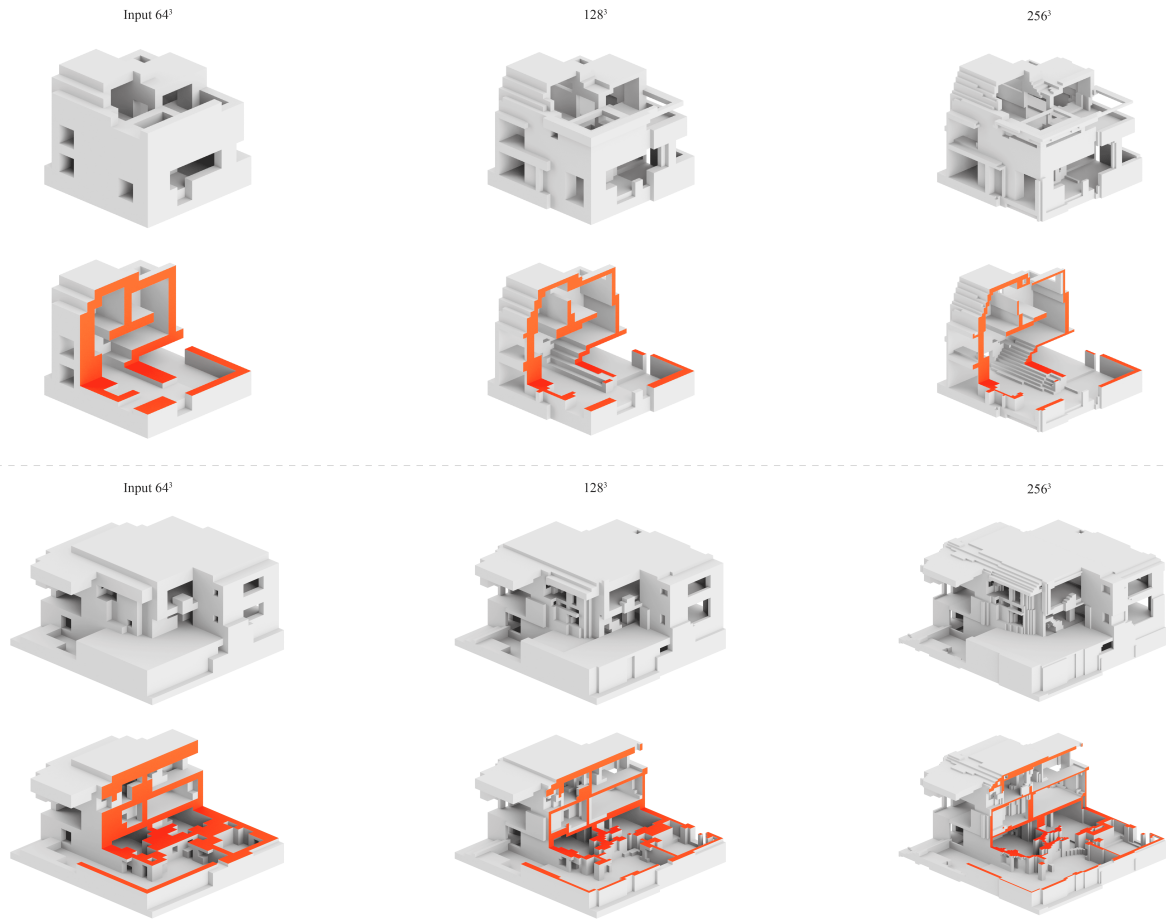
#### 5.1.4. Multi-Resolution Geometry Detailisation

To further support the designer with subsequent steps in volumetric design workflows, as outlined in Section 1, we utilise the hierarchy of 3D c-DDPMs to incrementally upsample the initial resolution of the output voxel grids of  $64^3$  to first  $128^3$  and then  $256^3$ , to augment the generated shapes with fine structures and geometric details. Since ArchComplete is scale consistent, this increase in resolution reflects a change of the true voxel size of 75cm to 18.75cm, indicating the degree of detail to which the upsampling process predicts new spatial elements and features (see Figure 10).

## 5.2. Evaluation and Comparison

We thoroughly evaluate our network design and choice of parameters, and compare our results quantitatively and qualitatively in both unconditional and conditional synthesis tasks to two of the state-of-the-art methods.

We compare ArchComplete to the 3D generative models SDFusion [CLT\*23] and NWD [HLHF22], due to slight similarities in their geometric representations and network designs. Both methods also use dense voxel grids to represent the data as Truncated Signed Distance Fields (TSDFs), where individual voxels, instead of binary occupancy values, store scalar distances to the nearest surface. Like our base network’s quantisation step, SDFusion leverages a 3D-variant of VQVAE to compress the 3D shape into a



**Figure 10:** Two levels of the detailisation process showcasing how upsampling networks refine mass, introducing openings and elements while thinning walls and floors to achieve accurate architectural thickness.

lower-dimensional compact discrete latent space. WaveGen is also a two-stage pipeline: a generator for coarse shape generation, followed by a diffusion-based *detail predictor* for enriching the generated shapes with fine structures and details, similar to our upsampling networks.

We train both methods—SDFusion for 128 epochs (including its diffusion models for 256 epochs) and NWD [HLHF22] for its preset epochs—on our dataset using the exact same network architecture and parameters as in their original implementations. To ensure consistency, we extract the SDF values at the resolution of our binary voxel grids ( $64^3$ ) for training, and for inference, we voxelise the corresponding resultant surface meshes at this resolution for comparison.

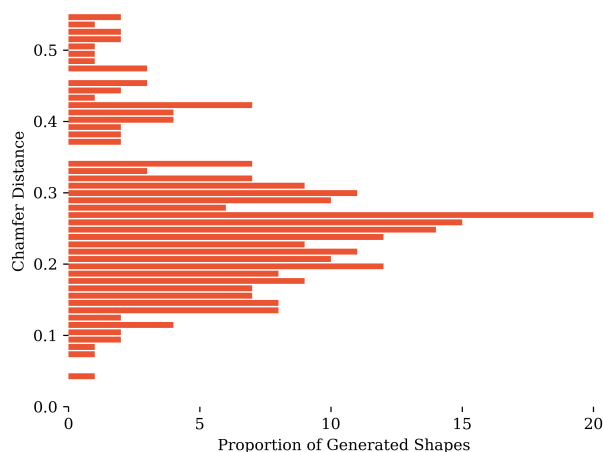
### 5.2.1. Unconditional: Shape Novelty Analysis

Evaluating the unconditional synthesis of 3D shapes presents challenges due to the absence of direct ground truth correspondence. To address this, we adopt a two-fold evaluation approach: first, we assess the novelty of our generated shapes, and second, we measure

our method’s performance in terms of shape quality to the other two existing works.

First, we evaluate whether our method can generate novel shapes in unconditional synthesis tasks to ensure that the model is not merely retrieving existing shapes from the training dataset. Following the methodology in previous works [EMS\*23, SAA\*24], we generate 256 shapes using our base network. For each generated shape, we identify the top five nearest neighbours from the training set based on Chamfer Distance (CD) and plot the distribution of generated house models and their closeness to training distribution. As depicted in Figure 11, the CD distribution reveals that our method not only covers shapes in the training set, indicated by low CD values, but also successfully generates novel and realistic-looking house models (see Figures 8 and 12), as indicated by high CD values.

Next, to assess the model’s performance in comparison to state-of-the-art methods, we generate an equal number of shapes using two other methods from the literature and assess them un-



**Figure 11:** Shape novelty analysis on our dataset of 3D house models. Our pipeline can generate shapes that are similar (low CD) as well as different (high CD) from the training distribution, with shapes at the 50th percentile different from closest train shape.

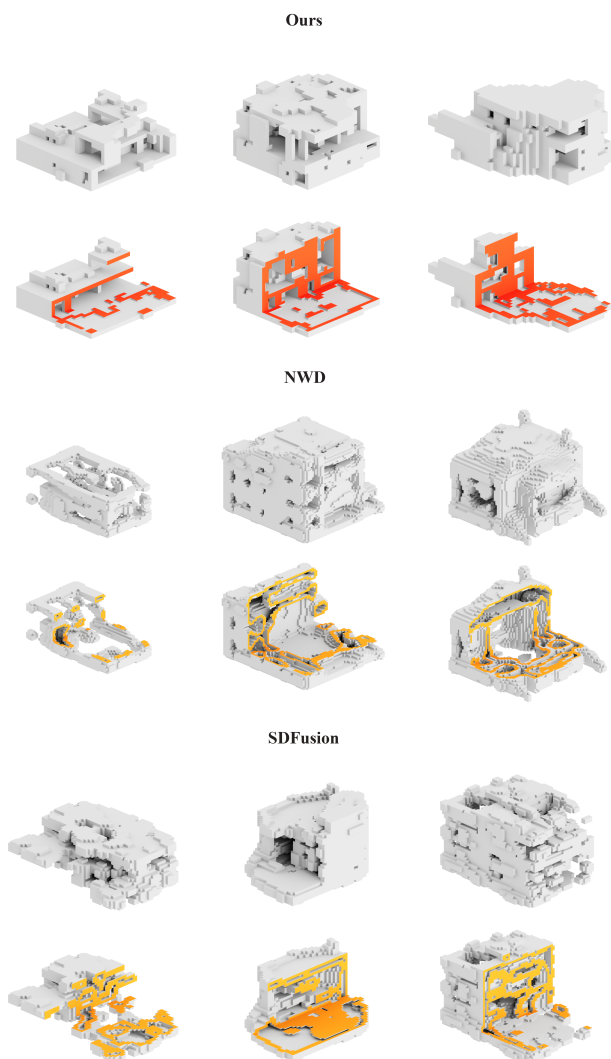
der three criteria: Minimum Matching Distance (MMD), Coverage (COV), and 1-Nearest-Neighbor Accuracy (1-NNA). Similar to above, herein we also use CD measure for computing these metrics in 3D. As outlined in Figure 12 and Table 1 our method outperforms both [HLHF22] and SDFusion by creating house models with more intricate geometric details and significantly fewer artifacts and noise while producing architecturally more sound and structured interior spaces of varying sizes. We attribute this to two main factors: first, in resolution of  $64^3$  binary voxel grid data representation, represents the geometry with higher precision, than TSDF. The truncation threshold in SDF results in voxels that extend beyond the geometry’s original surface; and second, our tailored approach to house models, integrating a 2.5D perceptual loss during training enables the model enhances the model’s understanding of house models. This makes it superior to methods such as NWD and, which are better suited for more common objects in benchmarks like ShapeNet, consisting of objects with less intricate geometric details.

Method	COV $\uparrow$	MMD $\downarrow$	1-NNA
NWD [HLHF22]	35.00	0.85	81.93
SDFusion [CLT*23]	30.50	0.83	85.54
Ours	<b>74.50</b>	<b>0.25</b>	<b>75.51</b>

**Table 1:** Quantitative comparison on the task of unconditional mesh generation. For MMD, lower is better; for COV, higher is better; for 1-NNA, 50% is the optimal. We outperform the baselines on the shape quality metrics.

### 5.2.2. Conditional: Shape Fidelity and Diversity

We also quantitatively and qualitatively assess and measure the performance of our approach on the task of shape completion both in terms of fidelity and diversity. To this end, given partial input



**Figure 12:** Qualitative comparison of the unconditional synthesis task against NWD [HLHF22] and SDFusion [CLT\*23]. Compared to the baselines, our pipeline produces 3D house models with higher geometric fidelity, showcasing both exteriors and interiors with well-defined, architecturally reasonable closed and open spaces.

shapes, we generate  $k$  complete shapes. To measure the completions’ fidelity given a partial input, we compute the average of *Unidirectional Hausdorff Distance (UHD)* to the  $k$  generated shapes. Correspondingly, given the  $k$  generated results for each shape, we compute the average CD to other  $k - 1$  shapes; The sum of the average distance among  $k$  generation indicates the completion diversity and is denoted as *Total Mutual Difference (TMD)*. We use  $k = 10$  in our evaluations and report these metrics on our dataset, as shown in Table 2.

Method	UHD ↓	TMD ↑
SDFusion [CLT*23]	0.0572	0.1252
Ours	<b>0.0398</b>	<b>0.2535</b>

**Table 2:** Quantitative comparison of conditional synthesis: shape completion results. We evaluate our method’s fidelity (UHD) and diversity (TMD) in comparison to [HLHF22] and SDFusion [CLT\*23] trained on our dataset.

### 5.2.3. Runtime and GPU Memory

Generally, one critical limitation when upsampling dense voxel grids to higher resolutions, e.g.,  $256^3$  ( $512^3$ ), is the long runtime and the (severe) usage or overflow of GPU memory. Our proposed hierarchical upsampling networks process the input voxel grids locally, i.e., chunk-by-chunk, hence drastically reducing runtime and memory requirements. This is achieved by unfolding the coarse  $64^3$  voxel grids to  $8^3$  and  $16^3$  chunks, upsampling them to  $16^3$  and  $32^3$ , that when folded back from  $128^3$  and  $256^3$  fine grids, respectively.

To validate our method’s inference time and GPU footprint, we adopt the generator from the upsampling network architectures used in DECOR-GAN [CKF\*21] as a baseline. In their original implementation, the generator is designed to upsample  $X^3$  coarse voxel grids to  $(4X)^3$  while a style latent code is fed into the generator to condition the refinement to condition the upsampling on specific geometric styles. To ensure a fair comparison, we remove the final upsampling layer and adjust the input and output resolutions to  $(X)^3$  and  $(2X)^3$ , respectively, and drop the conditioning layers. The results are presented in Table 3, which shows that our model requires much less GPU memory and runs faster as the output resolution increases. Another key advantage is a direct benefit from additional supervision at intermediate-level resolution, which leads to higher-quality generation of finer scale geometric details.

Method	Output Resolution	Runtime (s)	Memory (GB)
DECOR-GAN	$64^3 \rightarrow 128^3$	1.27	6.68
ArchComplete		<b>0.83</b>	<b>1.36</b>
DECOR-GAN	$128^3 \rightarrow 256^3$	2.34	35.95
ArchComplete		<b>1.72</b>	<b>3.84</b>

**Table 3:** Resource computation comparison. HUN: Hierarchical Upsampling Networks, OOM: Out of Memory. Inference time is computed for the total 512 chunks in our hierarchical upsamplings.

## 6. Conclusion

We presented ArchComplete, a voxel-based autoregressive and hierarchical generative pipeline for 3D architectural modelling. In summary, our key contributions are as follows: We learn a vocabulary of local volumetric patch embeddings over a distribution of 3D voxelised house models through our tailored 3D Voxel VQGAN — with a new 2.5D perceptual loss term designed to capture the inherent complexity of input models — over which a transformer is trained to synthesise novel 3D house models in an autoregressive fashion. Moreover, our Hierarchical Voxel Upsampling Networks,

trained on local chunks instead of entire objects, can augment the outputs with rich geometric details (with a  $4X$  upsampling rate in our current implementation) and are significantly more efficient in terms of computational resources. We demonstrated several example applications enabled by our 3D generative pipeline, including blending and variation of input models, partial shape completion, and a domain-specific use case: synthesising 3D house models from 2D plan drawings as a form of shape completion. Furthermore, our evaluations revealed the capability of our pipeline in generating high-fidelity, 1:1 scale-consistent and diverse 3D house models that outperform state-of-the-art.

**Limitations and Future Work.** First and foremost, the dataset used in this study introduces constraints. While it enabled realistic and coherent generation of detailed architectural 3D models, its size and diversity were limited. This restricts the pipeline’s applicability across broader architectural styles and typologies, confining it to free-standing houses. Hence, expanding the dataset to include a wider variety of typologies could enhance the pipeline’s generalisation. By incorporating richer data metadata, e.g., texture or material information, into the voxelised models, the pipeline could be adapted to enable semantically segmented shape generation. Combining text descriptions of individual houses in the dataset with CLIP [RKH\*21] embeddings would enable image- and text-driven 3D generation, further expanding the pipeline’s interaction modes. While the hierarchical diffusion models successfully enhance geometric detail, error accumulation is inherent in our hierarchical upsamplings, where higher resolution grids cannot easily fix the artefacts from the prior levels. This problem can potentially be mitigated by appending refinement networks to each level in the hierarchy, which we leave for future work. Another limitation of our devised geometry detailisation is that it may sometimes lead to slight topological inconsistencies in the upsampled shapes as it lacks awareness to global structures. This issue could be addressed by adding a network branch to encode global shape properties and integrating it into the latent space of conditional diffusion models.

## References

- [ADMG18] ACHLIOPTAS P., DIAMANTI O., MITLIAGKAS I., GUIBAS L.: Learning representations and generative models for 3d point clouds. In *International conference on machine learning* (2018), PMLR, pp. 40–49. 2
- [BAG24] BAG D.: 3d bag, 2024. Accessed: 2024-10-09. URL: <https://3dbag.n1.3>
- [BDEW] BAUSCHER E., DAI A., ELSHANI D., WORTMANN T.: Learning and generating spatial concepts of modernist architecture via graph machine learning. 3
- [CCL\*21] CHANG K.-H., CHENG C.-Y., LUO J., MURATA S., NOUR-BAKHSH M., TSUJI Y.: Building-gan: Graph-conditioned architectural volumetric design generation. In *Proceedings of the IEEE/CVF international conference on computer vision* (2021), pp. 11956–11965. 2
- [CFG\*15] CHANG A. X., FUNKHOUSER T., GUIBAS L., HANRAHAN P., HUANG Q., LI Z., SAVARESE S., SAVVA M., SONG S., SU H., ET AL.: Shapenet: An information-rich 3d model repository. *arXiv preprint arXiv:1512.03012* (2015). 2
- [Che24] CHEREAU G.: Goxel: 3d voxel editor. <https://goxel.xyz/>, 2024. Accessed: 2024-11-11. 9
- [CKF\*21] CHEN Z., KIM V. G., FISHER M., AIGERMAN N., ZHANG

- H., CHAUDHURI S.: Decor-gan: 3d shape detailization by conditional refinement. In *Proceedings of the IEEE/CVF conference on computer vision and pattern recognition* (2021), pp. 15740–15749. [12](#)
- [CLT\*23] CHENG Y.-C., LEE H.-Y., TULYAKOV S., SCHWING A. G., GUI L.-Y.: Sdfusion: Multimodal 3d shape completion, reconstruction, and generation. In *Proceedings of the IEEE/CVF Conference on Computer Vision and Pattern Recognition* (2023), pp. 4456–4465. [2](#), [9](#), [11](#), [12](#)
- [Cro82] CROSS N.: Designly ways of knowing. *Design studies* 3, 4 (1982), 221–227. [3](#)
- [DMVPSC19] DE MIGUEL J., VILLAFANE M. E., PISKOREC L., SANCHO-CAPARRINI F.: Deep form finding using variational autoencoders for deep form finding of structural typologies. In *37th Conference on Education and Research in Computer Aided Architectural Design in Europe (eCAADe) & 23rd Conference of the Iberoamerican Society Digital Graphics (SIGraDi)* (2019), eCAADe, pp. 71–80. [3](#)
- [EMS\*23] ERKOÇ Z., MA F., SHAN Q., NIESSNER M., DAI A.: Hyperdiffusion: Generating implicit neural fields with weight-space diffusion. In *Proceedings of the IEEE/CVF international conference on computer vision* (2023), pp. 14300–14310. [10](#)
- [ERO21] ESSER P., ROMBACH R., OMMER B.: Taming transformers for high-resolution image synthesis. In *Proceedings of the IEEE/CVF conference on computer vision and pattern recognition* (2021), pp. 12873–12883. [2](#), [3](#), [4](#), [7](#)
- [GJvK20] GUAN Y., JAHAN T., VAN KAICK O.: Generalized autoencoder for volumetric shape generation. In *Proceedings of the IEEE/CVF Conference on Computer Vision and Pattern Recognition Workshops* (2020), pp. 268–269. [3](#)
- [HJA20] HO J., JAIN A., ABBEEL P.: Denoising diffusion probabilistic models. *Advances in neural information processing systems* 33 (2020), 6840–6851. [2](#), [3](#)
- [HLHF22] HUI K.-H., LI R., HU J., FU C.-W.: Neural wavelet-domain diffusion for 3d shape generation. In *SIGGRAPH Asia 2022 Conference Papers* (2022), pp. 1–9. [2](#), [3](#), [9](#), [10](#), [11](#), [12](#)
- [IZZE17] ISOLA P., ZHU J.-Y., ZHOU T., EFROS A. A.: Image-to-image translation with conditional adversarial networks. In *Proceedings of the IEEE conference on computer vision and pattern recognition* (2017), pp. 1125–1134. [4](#)
- [Kin13] KINGMA D. P.: Auto-encoding variational bayes. *arXiv preprint arXiv:1312.6114* (2013). [3](#)
- [Kin14] KINGMA D. P.: Adam: A method for stochastic optimization. *arXiv preprint arXiv:1412.6980* (2014). [7](#)
- [LDZL23] LI M., DUAN Y., ZHOU J., LU J.: Diffusion-sdf: Text-to-shape via voxelized diffusion. In *Proceedings of the IEEE/CVF conference on computer vision and pattern recognition* (2023), pp. 12642–12651. [3](#)
- [LH16] LOSHCHILOV I., HUTTER F.: Sgdr: Stochastic gradient descent with warm restarts. *arXiv preprint arXiv:1608.03983* (2016). [7](#)
- [LH21] LUO S., HU W.: Diffusion probabilistic models for 3d point cloud generation. In *Proceedings of the IEEE/CVF conference on computer vision and pattern recognition* (2021), pp. 2837–2845. [2](#)
- [Los17] LOSHCHILOV I.: Decoupled weight decay regularization. *arXiv preprint arXiv:1711.05101* (2017). [7](#)
- [LSC24] LEE H., SAVVA M., CHANG A. X.: Text-to-3d shape generation. In *Computer Graphics Forum* (2024), Wiley Online Library, p. e15061. [2](#)
- [LYF17] LIU J., YU F., FUNKHOUSER T.: Interactive 3d modeling with a generative adversarial network. In *2017 International Conference on 3D Vision (3DV)* (2017), IEEE, pp. 126–134. [2](#), [3](#)
- [MCST22] MITTAL P., CHENG Y.-C., SINGH M., TULSIANI S.: Autosdf: Shape priors for 3d completion, reconstruction and generation. In *Proceedings of the IEEE/CVF Conference on Computer Vision and Pattern Recognition* (2022), pp. 306–315. [2](#), [3](#)
- [PCN\*20] PERALTA D., CASIMIRO J., NILLES A. M., AGUILAR J. A., ATIENZA R., CAJOTE R.: Next-best view policy for 3d reconstruction. In *Computer Vision–ECCV 2020 Workshops: Glasgow, UK, August 23–28, 2020, Proceedings, Part IV 16* (2020), Springer, pp. 558–573. [3](#)
- [PIL\*21] PENG S., JIANG C., LIAO Y., NIEMEYER M., POLLEFEYS M., GEIGER A.: Shape as points: A differentiable poisson solver. *Advances in Neural Information Processing Systems* 34 (2021), 13032–13044. [3](#)
- [Rad18] RADFORD A.: Improving language understanding by generative pre-training. [5](#)
- [RFB15] RONNEBERGER O., FISCHER P., BROX T.: U-net: Convolutional networks for biomedical image segmentation. In *Medical image computing and computer-assisted intervention–MICCAI 2015: 18th international conference, Munich, Germany, October 5–9, 2015, proceedings, part III 18* (2015), Springer, pp. 234–241. [6](#)
- [RHZ\*24] REN X., HUANG J., ZENG X., MUSETH K., FIDLER S., WILLIAMS F.: Xcube: Large-scale 3d generative modeling using sparse voxel hierarchies. In *Proceedings of the IEEE/CVF Conference on Computer Vision and Pattern Recognition* (2024), pp. 4209–4219. [2](#), [3](#)
- [RKH\*21] RADFORD A., KIM J. W., HALLACY C., RAMESH A., GOH G., AGARWAL S., SASTRY G., ASKELL A., MISHKIN P., CLARK J., ET AL.: Learning transferable visual models from natural language supervision. In *International conference on machine learning* (2021), PMLR, pp. 8748–8763. [12](#)
- [RVdOV19] RAZAVI A., VAN DEN OORD A., VINYALS O.: Generating diverse high-fidelity images with vq-vae-2. *Advances in neural information processing systems* 32 (2019). [3](#)
- [SAA\*24] SIDDIQUI Y., ALLIEGRO A., ARTEMOV A., TOMMASI T., SIRIGATTI D., ROSOV V., DAI A., NIESSNER M.: Meshgpt: Generating triangle meshes with decoder-only transformers. In *Proceedings of the IEEE/CVF Conference on Computer Vision and Pattern Recognition* (2024), pp. 19615–19625. [2](#), [3](#), [10](#)
- [SCP\*23] SHUE J. R., CHAN E. R., PO R., ANKNER Z., WU J., WETZSTEIN G.: 3d neural field generation using triplane diffusion. In *Proceedings of the IEEE/CVF Conference on Computer Vision and Pattern Recognition* (2023), pp. 20875–20886. [3](#)
- [SHR23] SEBESTYEN A., HIRSCHBERG U., RASOULZADEH S.: Using deep learning to generate design spaces for architecture. *International Journal of Architectural Computing* 21, 2 (2023), 337–357. [3](#)
- [SME20] SONG J., MENG C., ERMON S.: Denoising diffusion implicit models. *arXiv preprint arXiv:2010.02502* (2020). [7](#)
- [SNL\*21] SELVARAJU P., NABAIL M., LOIZOU M., MASLIOUKOVA M., AVERKIOU M., ANDREOU A., CHAUDHURI S., KALOGERAKIS E.: Buildingnet: Learning to label 3d buildings. In *Proceedings of the IEEE/CVF International Conference on Computer Vision* (2021), pp. 10397–10407. [3](#)
- [SÖLH23] SEBESTYEN A., ÖZDENIZCI O., LEGENSTEIN R., HIRSCHBERG U.: Generating conceptual architectural 3d geometries with denoising diffusion models. In *Digital Design Reconsidered–Proceedings of the 41st Conference on Education and Research in Computer Aided Architectural Design in Europe (eCAADe 2023)–Volume* (2023), vol. 2, pp. 451–460. [3](#)
- [SSN\*22] SCHWARZ K., SAUER A., NIEMEYER M., LIAO Y., GEIGER A.: Voxgraf: Fast 3d-aware image synthesis with sparse voxel grids. *Advances in Neural Information Processing Systems* 35 (2022), 33999–34011. [2](#)
- [SZ14] SIMONYAN K., ZISSERMAN A.: Very deep convolutional networks for large-scale image recognition. *arXiv preprint arXiv:1409.1556* (2014). [5](#)
- [VDOV\*17] VAN DEN OORD A., VINYALS O., ET AL.: Neural discrete representation learning. *Advances in neural information processing systems* 30 (2017). [3](#)
- [VWG\*22] VAHDAT A., WILLIAMS F., GOJCIC Z., LITANY O., FIDLER S., KREIS K., ET AL.: Lion: Latent point diffusion models for 3d

- shape generation. *Advances in Neural Information Processing Systems* 35 (2022), 10021–10039. [3](#)
- [WDL\*23] WANG A., DONG J., LEE L.-H., SHEN J., HUI P.: Towards ai-architecture liberty: A comprehensive survey on designing and collaborating virtual architecture by deep learning in the metaverse. *arXiv preprint arXiv:2305.00510* (2023). [3](#)
- [WLY\*24] WU Z., LI Y., YAN H., SHANG T., SUN W., WANG S., CUI R., LIU W., SATO H., LI H., ET AL.: Blockfusion: Expandable 3d scene generation using latent tri-plane extrapolation. *ACM Transactions on Graphics (TOG)* 43, 4 (2024), 1–17. [3](#)
- [WSH\*18] WANG H., SCHOR N., HU R., HUANG H., COHEN-OR D., HUANG H.: Global-to-local generative model for 3d shapes. *ACM Transactions on Graphics (TOG)* 37, 6 (2018), 1–10. [3](#)
- [WZ22] WU R., ZHENG C.: Learning to generate 3d shapes from a single example. *arXiv preprint arXiv:2208.02946* (2022). [3](#)
- [Yuk15] YUKSEL C.: Sample elimination for generating poisson disk sample sets. In *Computer Graphics Forum* (2015), vol. 34, Wiley Online Library, pp. 25–32. [4](#)
- [ZKF23] ZHONG X., KOH I., FRICKER P.: Building-gnn: Exploring a co-design framework for generating controllable 3d building prototypes by graph and recurrent neural networks. In *International Conference on Education and Research in Computer Aided Architectural Design in Europe* (2023), eCAADe, pp. 431–440. [3](#)